Nuclear fission of neutron-deficient protactinium nuclides

I. Nishinaka, Y. Nagame, K. Tsukada, and H. Ikezoe
Japan Atomic Energy Research Institute, Tokai-mura, Naka-gun, Ibaraki 319-11, Japan

K. Sueki and H. Nakahara
Faculty of Science, Tokyo Metropolitan University, Minami-Ohsawa, Hachioji, Tokyo 192-03, Japan

M. Tanikawa
School of Science, University of Tokyo, Hongo, Bunkyo-ku, Tokyo 113, Japan

T. Ohtsuki
Laboratory of Nuclear Science, Tohoku University, Mikamine, Taihaku-ku, Sendai 982, Japan
(Received 12 March 1997)

Fragment velocity, kinetic energy, mass yield, and element yield distributions in the fission of neutron-deficient Pa isotopes produced in the reactions of ^{16}O and ^{18}O on ^{209}Bi have been measured at incident beam energies near and above the Coulomb barriers by the time-of-flight and radiochemical methods. An asymmetric mass-division component has been observed. Measured fission cross sections were compared with the results of statistical model calculations which take into account two fission barrier heights for symmetric and asymmetric yields. The fission barrier height deduced for the asymmetric fission is found slightly lower than that for the symmetric one. The difference between the two barrier heights in the fission of the present protactinium nuclides ($N\sim135$) is considerably smaller than that in the neutron-rich nuclide of ^{233}Pa ($N\sim142$), indicating that the difference sensitively depends on the neutron number of the fissioning nuclide. [S0556-2813(97)03708-4]

PACS number(s): 25.85.Ge

I. INTRODUCTION

Symmetric and asymmetric mass-division phenomena are the most puzzling feature of nuclear fission and a large number of data have been accumulated on mass yield distributions of fission fragments in relation to atomic number, mass number, and excitation energy of fissioning nuclides. General features of mass division phenomena in nuclear fission until 1971 could be summarized as the following: (1) Asymmetric mass division is predominant in low energy fission, spontaneous fission, and thermal-neutron induced fission of actinide nuclides. (2) Mass yield curves of fission fragments induced by light particles (p, α, and so on) in the radium region show three-humped shapes [1,2], while those of particle induced fission of the nuclides lighter than radium show mainly single peaks [3]. (3) Symmetric fragment yields increase more rapidly than asymmetric ones as the energy of incident particles is increased.

Such a picture has been further advanced by the recent studies for spontaneous fission of the heavy actinides and transactinides. Balagna *et al.* [4] first reported the presence of symmetric mass division and a very high total kinetic energy (TKE) component in the spontaneous fission of ^{257}Fm. Since then, mass yield curves of spontaneous fission of many heavy actinides have been investigated and the strong dependence of mass division phenomena on the number of neutrons and protons of the fissioning nuclides has been unveiled [5]. Hulet *et al.* [6] observed two kinds of scission configurations even for the same mass division and named such phenomena ''*bimodal fission.*'' Ohtsuki *et al.* [7] also observed such bimodal phenomena even in the fission of light actinides. Then, Nagame *et al.* [8] experimentally verified from the measurement of the correlation of the yield of each kinetic energy component with the excitation energy of the compound nucleus that two independent fission paths exist in the course of deformation from saddle to scission: one path leading to symmetric mass division with elongated scission configuration and the other leading to asymmetric mass division with more compact scission configuration.

The presence of such fission paths was first postulated by Turkevich and Niday as a hypothesis in 1951 [9], and many investigators have tried to verify it experimentally [2,10–12]. It is probable that such fission paths are critically influenced by the shell structure of a nucleus in the course of deformation. Möller has pointed out that the barrier height of the reflection asymmetric saddle is largely affected by the neutron shell structure [13].

From detailed studies of excitation functions of fission products, it is experimentally shown that the difference of barrier heights or threshold energies related to the asymmetric and symmetric mass division modes is more strongly affected by neutron number than proton number of fissioning nuclides, and that the difference decreases with the number of neutrons [14]. Strong influence of the neutron number of fissioning nuclides on mass division has been demonstrated in the spontaneous fission of heavy actinides [15]. However, as a whole, only a limited number of experimental data are available on the dependence of barrier heights on the neutron number [15,16]. As expected, the deformation path in fission is most sensitively affected by the potential energy surface and the effect of the neutron shell structure on fission can

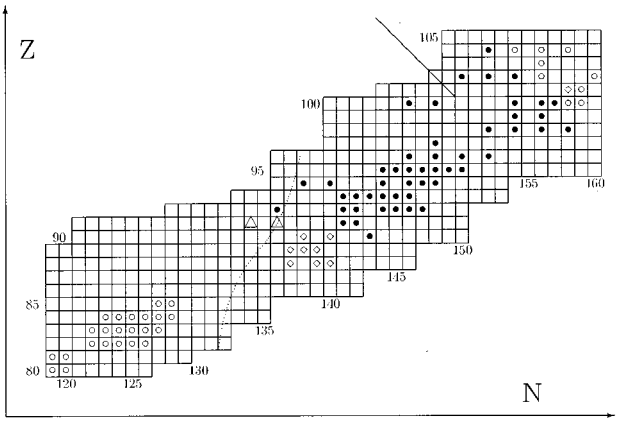

FIG. 1. A portion of the chart of nuclides. Closed and open circles show the nuclides for which the main mode of mass division in low energy fission is asymmetric and symmetric, respectively. Diamonds indicate the nuclides for which triple-humped mass yield curves were clearly observed [2,3,15–19,21–41]. Triangles show the compound nuclei studied in this work. The dotted line shows the region where the height of the reflection asymmetric barrier is expected to become comparable to that of the symmetric barrier according to the calculation in Ref. [13]. The thick line shows the region where the height of the reflection asymmetric barrier is expected to become comparable to the sum of the ground-state energy and a constant value of 0.5 MeV for the zero-point energy at the ground state as calculated in Ref. [52].

best be studied in spontaneous fission or in EC-delayed fission for some special nuclides [17–19]. However, no information can be obtained on the difference of the two fission barrier heights or on the difference in threshold energies from the study of spontaneous fission and it is accomplished only by use of low energy fission induced by light particles. Recently, Coulomb-excitation fission of neutron-deficient isotopes has been investigated by use of the secondary radioactive beam produced by projectile fragmentation of relativistic ^{238}U beams. However, in this new technique the excitation energy distribution of the Coulomb fission is quite large [20] and besides, it is difficult to extract the fission phenomena due purely to the Coulomb fission.

The aim of the present work is to study the degree of the contribution of asymmetric mass division in the low energy fission of neutron-deficient light actinides by observing yields of fission products in detail. Such results will help understand the influence of the nuclear structure of the fissioning nuclide on the mode of mass division in low energy nuclear fission, and, consequently, the process of large deformation of a nucleus toward fission. Mass yield distributions and kinetic energy distributions of fission fragments are measured by a time-of-flight (TOF) technique and element yield distributions by a radiochemical method for the light-heavy-ion induced reactions of ^{16}O, ^{18}O + ^{209}Bi, where the compound nuclei ^{225}Pa($N=134$) and ^{227}Pa($N=136$), respectively, are produced. The produced compound nuclei are located in the region of neutron-deficient light actinides where the height of the symmetric second barrier is expected to become comparable to that of the second barrier with reflection asymmetry according to Möller [13]. (See the dotted line in Fig. 1.)

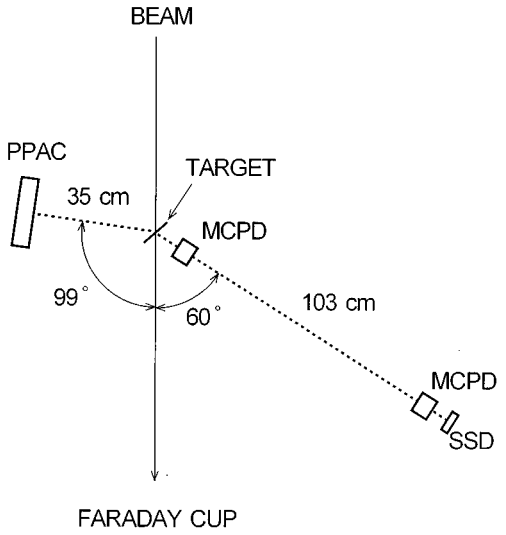

FIG. 2. Schematic view of the TOF experimental setup. For the details of the detectors shown by acronym, see text.

II. EXPERIMENTS

A. Time-of-flight experiments

Beams of ^{18}O with energies of 83 and 85 MeV and ^{16}O with 86 and 98 MeV were supplied from the JAERI tandem accelerator to bombard a ^{209}Bi target of about 40 μg/cm^2 thickness evaporated onto a carbon backing foil (10 μg/cm^2). A typical beam intensity was about 100 pnA. Fission fragments were detected with a TOF telescope at $\Theta_{\rm lab} = 60^{\circ}$ as shown in Fig. 2. Each start and stop detector (MCPD) [42,43] was composed of a carbon foil (20 μg/cm^2) and a couple of microchannel plates (MCP). Kinetic energies of fission fragments were measured by a 300 μg/cm^2 thick silicon surface barrier detector (SSD). The flight path from the start detector to the stop detector was 103 cm and the solid angle ($d\Omega$) of SSD was 0.3 msr. Complementary fragments were detected, in coincidence with the stop signal of TOF, by a position sensitive parallel plate avalanche counter (PPAC) whose solid angle was $d\Omega$ = 80 msr. The PPAC located on the opposite side of the beam direction at $\Theta_{\rm lab} = 99^{\circ}$ and at about 35 cm from the target. Calibrations of the time for the TOF system and the energy for the SSD were performed by measuring the elastically scattered ^{16}O and ^{18}O ions from a ^{209}Bi target, and also the particles recoiling out from thin targets, $^{\rm nat}$Ag (25 μg/cm^2), $^{\rm nat}$In (50 μg/cm^2), $^{\rm nat}$Sb (75 μg/cm^2) by bombardment of the 350 MeV ^{127}I beam. The pulse height defect and plasma delay of the SSD were estimated by the method proposed by Kaufman *et al.* [44] and Neidel *et al.* [45], respectively. The energy and time resolutions (FWHM) for the elastically scattered ^{16}O and ^{18}O ions were 0.2 MeV and 0.5 ns, respectively. The obtained overall mass resolution (FWHM) for the recoil product of $^{\rm nat}$In with 82 MeV (^{115}In 95.7%, ^{113}In 4.3%) recoils was 2.8 u.

B. Radiochemical experiments

The ^{209}Bi targets (each about 1 mg/cm^2 thick) were prepared by vacuum evaporation onto aluminium backing foils (5.4 mg/cm^2), and they were stacked into a target assembly

with aluminium catcher foils and aluminium energy degraders of appropriate thickness. Bombardments were carried out with energies of 107 and 115 MeV ^{16}O beams using the SF cyclotron at the Institute for Nuclear Study, University of Tokyo (INS) and with energies of 109 and 125 MeV ^{18}O using the JAERI tandem accelerator. Average beam currents were about 30–120 pnA. The irradiation duration was varied from 15 min to 2 h to ensure adequate radioactivities of fission products. The cross section of each product was determined by γ-ray spectrometry. The products of Sb, I, and Cs were chemically separated from other fission products before γ-ray measurements.

III. RESULTS AND DISCUSSION

A. Time-of-flight experiments

The number of fission coincidence events observed was 4.0×10^3, 2.8×10^4, 5.0×10^4, and 2.2×10^4 for the ^{18}O (83, 85 MeV) + ^{209}Bi, ^{16}O (86, 98 MeV) + ^{209}Bi, respectively. Figure 3 shows velocity ($v_{\mathrm{c.m.}}$) distributions in the center-of-mass system obtained from the TOF measurements with an assumption of full momentum transfer followed by fission. The velocity distributions observed for the reactions near the Coulomb barrier [Figs. 3(a), (c), and (d)] clearly exhibit the presence of some shoulder structure at around 0.048 in $v_{\mathrm{c.m.}}/c$ units. No clear fine structure was present in the kinetic energy ($E_{k\mathrm{c.m.}}$) distributions (Fig. 4) in the center-of-mass system observed by the SSD detector possibly due to smearing by the pulse height defect and neutron emission from primary fragments.

Figure 5 shows mass (m) yield curves of secondary fragments (post neutron emission) derived from the velocity (v_{lab}) and the kinetic energy ($E_{k\mathrm{lab}}$) in the laboratory system using the relationship $m=2E_{k\mathrm{lab}}/v_{\mathrm{lab}}^2$. As tabulated in Table I, the observed mean mass number of secondary fragments shows that the sum of average number of neutrons emitted before and after fission is 5.6 and 7.2 in the 86 MeV and 98 MeV ^{16}O induced reactions, and 6.6 and 6.4 in the 83 MeV and 85 MeV ^{18}O induced reactions, respectively. The secondary mass yield curves are nearly symmetric and can be fitted as a first approximation by a Gaussian function with the standard deviation of $\sigma_A=14.3$–15.6 u, but the presence of some asymmetric components, especially in the mass yield curves of the ^{18}O + ^{209}Bi reaction, are clearly observed at around the mass numbers 88 and 132.

Primary fragment mass (m^*) was obtained by correcting for neutron emission from primary fragments as explained in the following. The total excitation energy available for a pair of primary fragments before neutron emission (E_f^*) is given by the following equation:

$$E_f^*=E_{\mathrm{CN}}^*+Q_{gg}-\mathrm{TKE}, \tag{3.1}$$

where E_{CN}^*, Q_{gg}, and TKE are the excitation energy of the compound nucleus, the ground-state Q value for producing the pair, and the total kinetic energy of the pair fragments, respectively. Here, no neutron emission prior to fission is assumed. For calculating Q_{gg} for a certain mass division, the atomic mass table [46,53] by assuming the UCD (unchanged charge distribution) hypothesis for the most-probable charge.

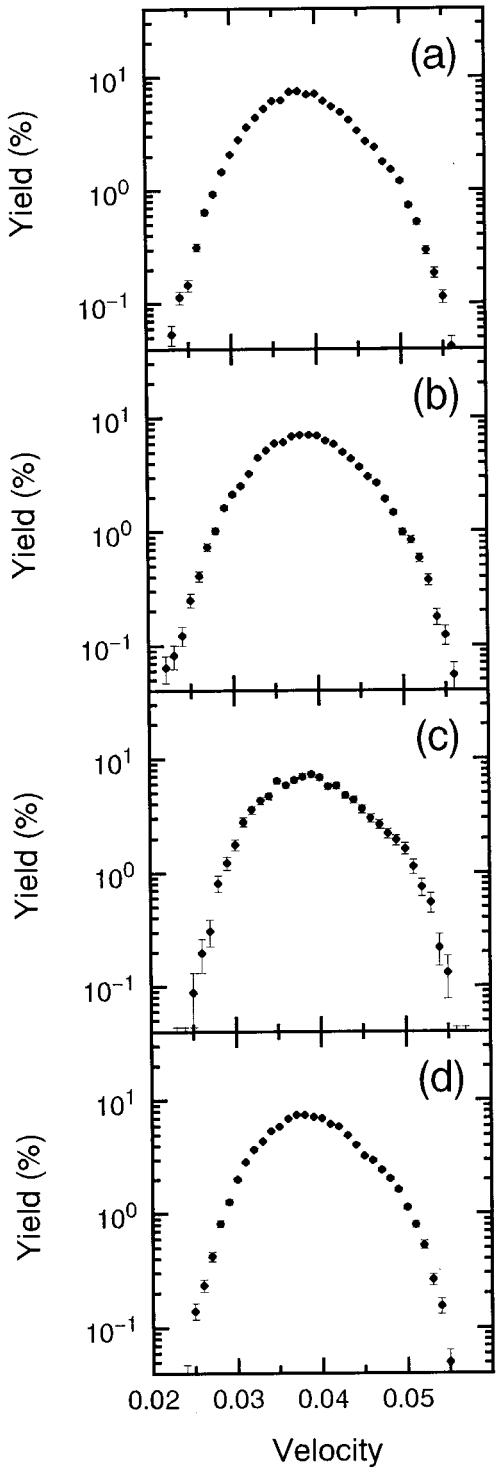

FIG. 3. Velocity distributions of fission fragments in the center-of-mass system obtained for the ^{16,18}O + ^{209}Bi reactions: (a) 86 MeV ^{16}O, (b) 98 MeV ^{16}O, (c) 83 MeV ^{18}O, and (d) 85 MeV ^{18}O.

If the total excitation energy (E_f^*) is shared between the complementary fragments in proportion to their masses, the fragment excitation energy (E^*) is given by

$$E^*=E_f^*\frac{m^*}{m_f}, \tag{3.2}$$

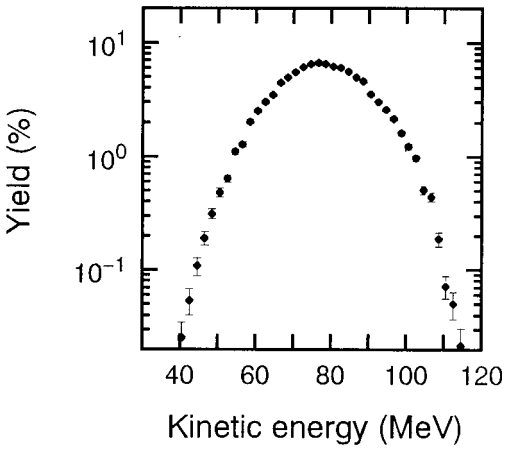

FIG. 4. Kinetic energy distributions of fission fragments in the center-of-mass system for the 85 MeV ^{18}O + ^{209}Bi reaction.

where m_f denotes the mass number of the fissioning nuclide. Although the average mass of the fissioning nuclide was unknown in the present reactions, m_f was assumed to be equal to the mass number of the compound nucleus since the estimated primary mass yield curves were not affected much by the assumed number of prefission neutrons unless mass division phenomena drastically changed as the fissioning nuclide was varied. E^* is then dissipated through the emission of neutrons and γ rays from primary fragments,

$$E^* = \Sigma_{i=1}^{\overline{\nu_i}}(B_{ni} + \epsilon_{ni}) + E_\gamma, \tag{3.3}$$

where $\overline{\nu_i}$, B_{ni}, ϵ_{ni}, and E_γ indicate the number of neutrons emitted, separation energy and kinetic energy of the ith neutron, and the energy released as γ rays. The number of the emitted neutrons is estimated from Eq. (3.3) by assuming B_{ni} = 8 MeV, ϵ_{ni} = 2T, and E_γ = 4 MeV. The temperature of the fission fragment T is given by

$$T = \sqrt{8E^*/m^*}. \tag{3.4}$$

Mass (m^*) and kinetic energy (E_k^*) of a primary fragment are evaluated by

$$m^* = m + \overline{\nu_i}, \tag{3.5}$$

$$E_k^* = \frac{1}{2} m^* v_{\text{c.m.}}^2. \tag{3.6}$$

Here, it is assumed that neutrons are isotropically emitted from the primary fragment and do not alter the initial fragment velocity on average. The total kinetic energy of fragments before neutron emission is then evaluated by

$$\text{TKE} = E_k^* \frac{m_f}{m_f - m^*}. \tag{3.7}$$

The above calculations were reiterated for each observed fission event until convergence of the primary mass was attained.

The primary mass yield curves thus obtained are shown in Fig. 6. They are approximately symmetric around half of the compound mass number and can be well fitted by three Gaussians. By setting the Gaussian parameters of the height and width being equal for the light and heavy asymmetric components, as they should be, asymmetric peaks centered around the mass numbers of 90 and 137 were deduced as shown in the figures by short-dashed curves. The relative yield of the asymmetric component is about 10% of the total fission yield at the compound excitation energy of 32 MeV in both ^{16}O and ^{18}O reactions.

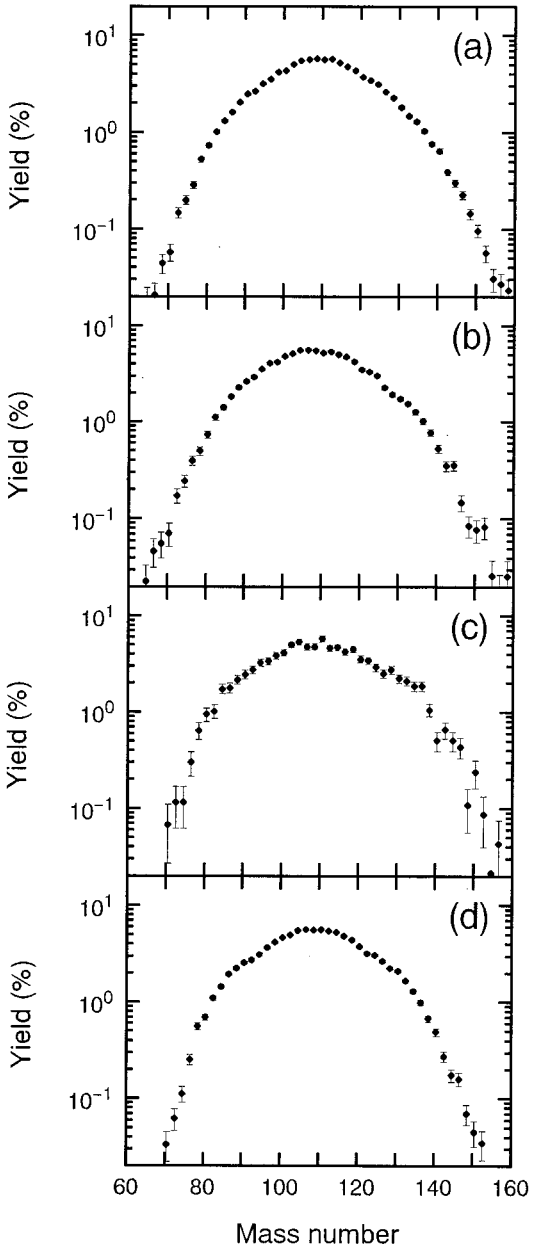

FIG. 5. Mass yield distributions of secondary fission fragments in the ^{16,18}O + ^{209}Bi reactions: (a) 86 MeV ^{16}O, (b) 98 MeV ^{16}O, (c) 83 MeV ^{18}O, and (d) 85 MeV ^{18}O.

After correction for neutron emission, the overall average of TKE was obtained to be 162 MeV which was about 6 MeV smaller than that predicted by the systematics of Viola *et al.* [47].

TABLE I. Average values and standard deviations of velocity ($v_{\mathrm{c.m.}}$) distributions, fragment kinetic energy ($E_{k\mathrm{c.m.}}$) distributions in the center-of-mass system and mass yield curves of secondary fragments, and distributions of total kinetic energy and mass yields of primary fragments evaluated after correction for neutron emission (E^*_{CN}, excitation energy of the compound nucleus; E_{lab}, incident particle energy; TKE, total kinetic energy of primary fragments).

Compound nucleus	E_{lab} MeV	E^*_{CN} MeV	$\overline{v_{\mathrm{c.m.}}}$ /c	$\sigma(v_{\mathrm{c.m.}})$ /c	$\overline{E_{k\mathrm{c.m.}}}$ MeV	$\sigma_{E_{k\mathrm{c.m.}}}$ MeV	$\overline{m_{\mathrm{sec}}}$ u	$\sigma(m_{\mathrm{sec}})$ u	$\overline{\mathrm{TKE}}$ MeV	σ_{TKE} MeV	$\overline{m_{\mathrm{pri}}}$ u	$\sigma(m_{\mathrm{pri}})$ u
^{225}Pa	86	32	0.0392	0.0055	77.9	12.2	109.7	14.1	161.4	11.9	112.9	14.4
^{225}Pa	98	44	0.0393	0.0056	77.8	12.6	108.9	14.2	161.5	12.5	112.7	14.6
^{227}Pa	83	30	0.0393	0.0056	77.8	12.3	110.2	15.4	162.0	10.2	113.2	15.6
^{227}Pa	85	32	0.0394	0.0053	78.9	11.9	110.3	14.0	162.8	11.3	113.6	14.3

B. Radiochemical Experiments

Typical cross sections of fission products obtained by the radiochemical method are plotted in Fig. 7 as a function of fragment mass number. Solid circles show the observed cross sections that are expected to represent the cumulative yields of respective mass chains and open circles show those representing independent or fractional cumulative yields in mass chains. Cumulative mass yields observed in the present experiment are very limited to the lighter side of the mass yield curve, because the most-probable charge of the isobaric yield distribution lies close to the β-stability line in heavy-ion induced fission.

In the present work, isotopic distributions of Sb($Z=51$), I ($Z=53$), and Cs($Z=55$) were obtained by observing independent fission yields (independent of the β-decay precursors). Then, they were converted into mass yield curves with the following reasonable assumptions: (i) isotopic distributions are of a Gaussian shape, (ii) isotopic yield distributions for the neighboring even elements $Z=50$, 52, 54, 56, can be constructed by estimating their Gaussian parameters of the width and the most probable mass number from the parameters observed for Sb, I, and Cs by interpolation and extrapolation. In the fission of 84 MeV ^{18}O + ^{209}Bi reaction, the average value of the width parameter is about 1.5 and the ratio of the atomic number (Z) to the most probable mass number (A_p) is 0.412, 0.411, and 0.410 for Sb, I, and Cs, respectively. Results are shown in Fig. 8. The even-odd effects of protons and neutrons on the isotopic yield distributions, which are known to be present in spontaneous fission and in thermal-neutron fission [48,49], are not considered in the present analysis since such effects are expected to be washed out in the fission of higher excitation energy. The mass yields are obtained by summing the yields of nuclides with the same mass number as shown in Fig. 8, and they are depicted by the thick lines in Fig. 7 for the fragment mass of 120–137. The secondary mass yield distributions observed by the TOF experiments are also indicated in the figures by dashed lines. They are normalized to the radiochemical data shown by solid points. As shown in Figs. 7(a) and 7(c), the shoulder structure around mass number 133 is noticeable in the curves constructed from the isotopic distributions.

The element yields which are unaffected by post-fission neutron emission can be obtained by summing over the isotopic yield distributions shown in Fig. 8. They are plotted in Fig. 9 for the fission of 85 MeV ^{18}O + ^{209}Bi reaction as a function of atomic number. Although the yields of only three

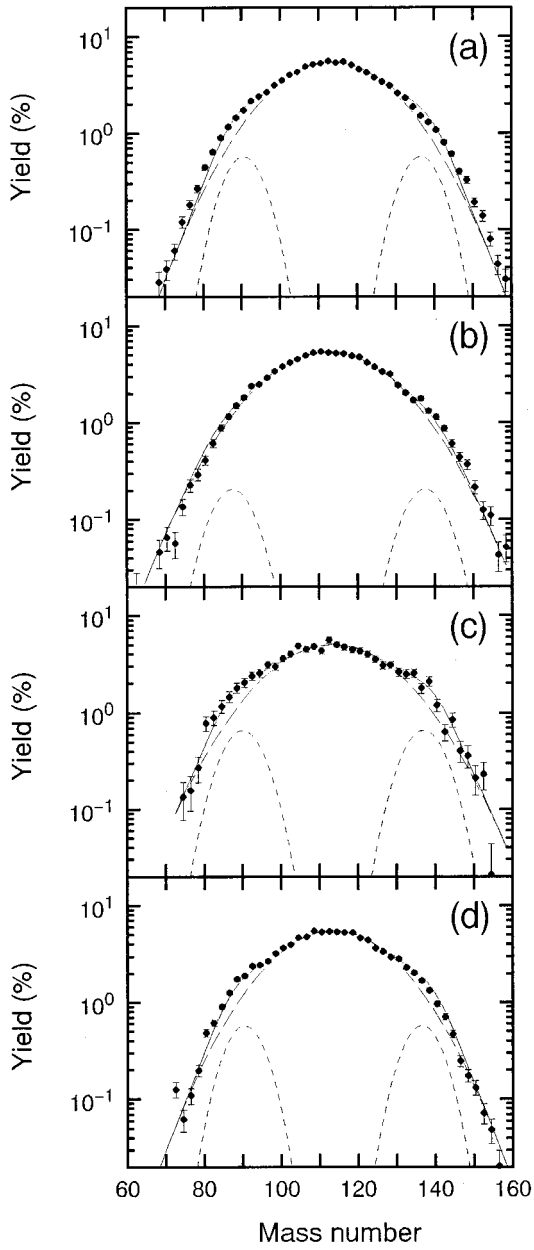

FIG. 6. Mass distributions of primary fission fragments in the ^{16,18}O + ^{209}Bi reactions: (a) 86 MeV ^{16}O, (b) 98 MeV ^{16}O, (c) 83 MeV ^{18}O, and (d) 85 MeV ^{18}O. The long-dashed and short-dashed lines obtained by three-Gaussian fitting show the symmetric and asymmetric components, respectively.

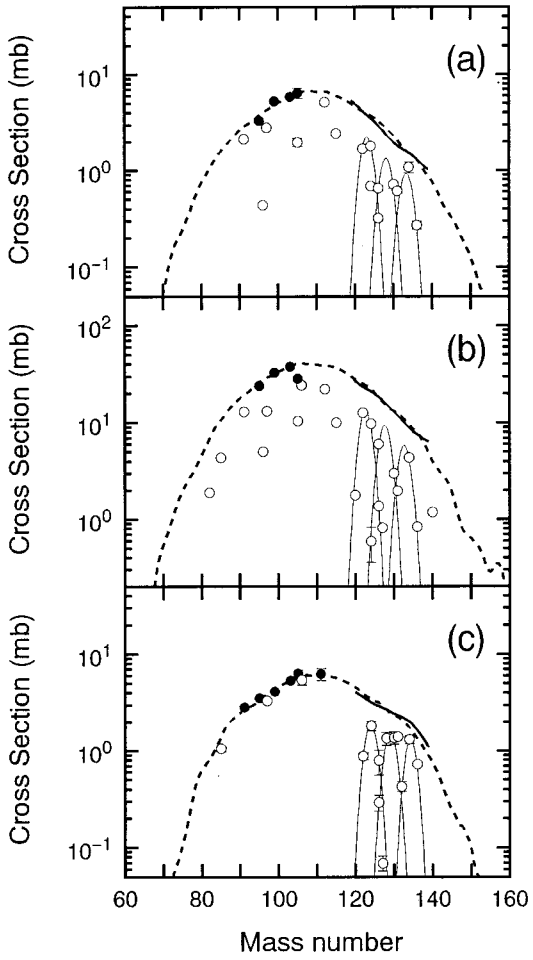

FIG. 7. Mass yields of secondary fragments in the $^{16,18}O + ^{209}Bi$ reactions: (a) 86 MeV ^{16}O, (b) 98 MeV ^{16}O, and (c) 84 MeV ^{18}O. Solid and open circles show the cumulative and the independent yields in each mass chain observed by the radiochemical experiments. The thin solid lines indicate isotopic distributions of Sb ($Z=51$), I ($Z=53$), and Cs ($Z=55$). The thick solid lines are the mass yield curves constructed from the isotopic distributions. The dashed lines show the secondary mass yield curves observed by the TOF experiments [(a) 86 MeV ^{16}O, (b) 98 MeV ^{16}O, and (c) 85 MeV ^{18}O] which are normalized to the radiochemical yield data shown by solid circles.

elements were observed in this work, the contribution of the asymmetric component can be estimated by the Gaussian curve fitting with the following assumptions: (i) the width of the element yield curve σ_Z of the symmetric charge division component can be approximated by

$$\sigma_Z = \sigma_A \frac{Z_p}{A_p}, \tag{3.8}$$

where σ_A is the width of the primary mass yield curve shown in Fig. 6, and (Z_p/A_p) is the charge density calculated by the UCD approximation. (ii) The width of the asymmetric component in the element yield curve can be estimated using the above equation with σ_A of the asymmetric Gaussian shown by short-dashed curves in Fig. 6. (iii) The peak position of the symmetric component in the element yield curve is fixed at $Z=45.5$ as it should be. (iv) The sum of the areas of two

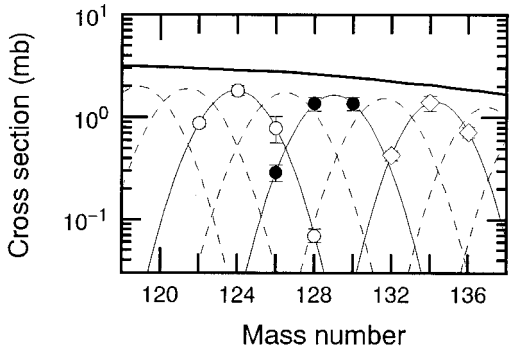

FIG. 8. Isotopic distributions observed in the fission of 84 MeV $^{18}O + ^{209}Bi$: ○ (Sb), ● (I), and ◇ (Cs). Thin solid lines show Gaussian curves fitted to the experimental data and the dashed lines are those whose Gaussian parameters were obtained by interpolation or extrapolation of the parameters deduced from the thin solid lines fitting to Sb, I, and Cs data points. The thick line shows mass yields obtained by summing over independent yields of the same mass number with different atomic numbers.

Gaussians is equal to the fission cross section obtained from Fig. 7, namely, by normalizing the TOF mass yield curves to the radiochemical data shown by solid points. Then the two-Gaussian analysis for the element yield distribution was carried out by allowing the remaining three parameters, the peak heights of the symmetric and asymmetric components and the peak position of the asymmetric component determined by fitting. The result is shown in Fig. 9 by the solid and short-dashed lines for the symmetric and asymmetric components, respectively. The percentage of the asymmetric component to the total fission yield is about 10% for the 84 MeV $^{18}O + ^{209}Bi$ system, and it is consistent with the result of the three-Gaussian fitting to the primary mass yield data for the 85 MeV $^{18}O + ^{209}Bi$ system shown in Fig. 6. The most probable atomic number of the asymmetric component

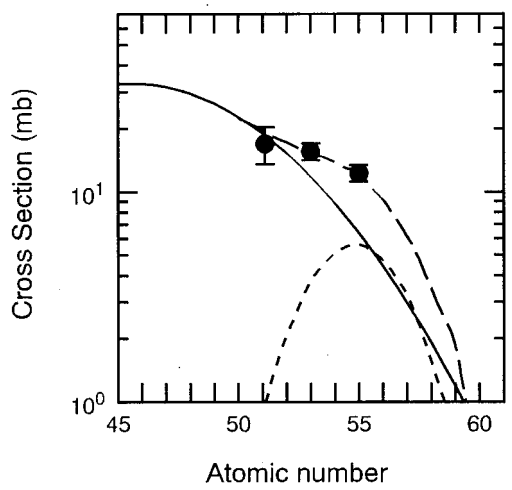

FIG. 9. Element yield distributions as a function of atomic number in the 84 MeV $^{18}O + ^{209}Bi$ reaction. The solid and short dashed lines show Gaussian curves for the symmetric and the asymmetric component, respectively. The long-dashed line is the sum of the two components. The widths of Gaussian curves are derived from the mass yield curves shown in Fig. 6.

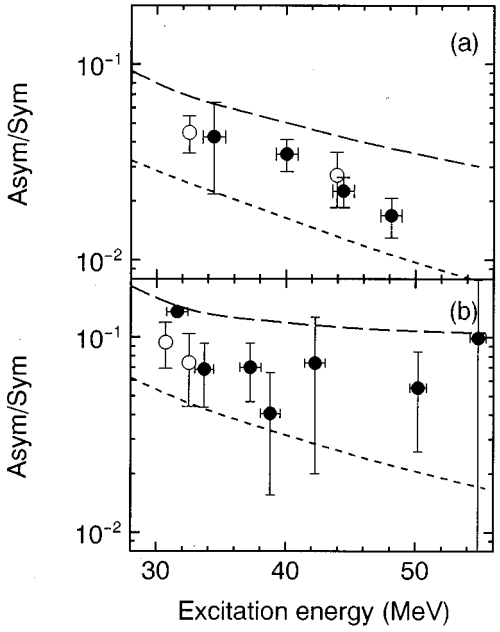

FIG. 10. The ratio of the asymmetric component yield to the symmetric yield as a function of the excitation energy in the (a) ^{16}O + ^{209}Bi and (b) ^{18}O + ^{209}Bi systems. The open and solid circles indicate the results from the TOF experiment and the radiochemical one, respectively. The results of the statistical calculation are shown by long-dashed and short-dashed lines for (a) $B_{f,a}$ = 4.4 and 5.3 MeV and (b) $B_{f,a}$=4.0 and 4.9 MeV.

obtained by fitting is 55 (see Fig. 9) which corresponds to the fragment neutron number of $N\sim82$ with $A\sim137$ if the UCD approximation is applied.

C. Incident energy dependence of asymmetric-to-symmetric yield ratio

Figure 10 shows the yield ratios of the asymmetric component to the symmetric one as a function of the excitation energy. Two components were evaluated from the Gaussian fitting of the primary mass yield curves obtained from the TOF experiments (open symbols) and the element yield curves observed by the radiochemical experiments (solid symbols). The errors in Fig. 10 are those associated with the fitting. The decreasing behavior of this ratio with the excitation energy is similar to that generally observed in the light particle induced fission of actinides [14] in which symmetric fission becomes more favored at higher incident energies. The statistical model calculation with the modified Alice code [37] which includes two competing fission channels with symmetric and asymmetric fission barriers was carried out. Details of this calculation are described in Ref. [14].

In the fitting procedure, the parameters used were as follows; $A/8$ for the level density parameter a_n for neutron emission, $a_{f,a}/a_n$=1.02 for the ratio of the level density parameters for asymmetric fission $a_{f,a}$ to a_n and $a_{f,s}/a_{f,a}$= 1.15 for symmetric fission $a_{f,s}$ to $a_{f,a}$. Extracted barriers must be dependent on the ratio of $a_{f,s}/a_{f,a}$ which cannot be determined as the free parameter from the experimental data by the calculation. However, the values of $a_{f,s}/a_{f,a}$ deduced from the proton induced fissions of ^{232}Th, ^{233}U, ^{235}U, ^{236}U, ^{238}U, ^{237}Np, ^{239}Pu, ^{242}Pu, and ^{241}Am are reported as 1.14–1.16 [14] to reproduce the excitation functions of the symmetric and asymmetric products, and the peak-to-valley ratios of the mass yield distributions. This choice of level density parameters is qualitatively in agreement with the earlier observation by Gavron *et al.* [50]. Therefore, we fixed the parameters as $a_{f,s}/a_{f,a}$=1.15. The finite range rotating liquid drop barrier [51], $B_{f,s}$=5.0 MeV, was used for the symmetric fission barrier in the ^{16}O + ^{209}Bi reaction. The calculation was carried out by varying only one parameter of the asymmetric fission barrier height. For reproducing the results of the present work, the asymmetric fission barrier had to be within the range of $B_{f,a}$=4.4–5.3 MeV, as shown in Fig. 10(a); the long-dashed and short-dashed lines are for $B_{f,a}$=4.4 and 5.3 MeV, respectively. In the ^{18}O + ^{209}Bi reaction the symmetric fission barrier of the finite range rotating liquid drop model [51] was $B_{f,s}$=5.1 MeV, and the asymmetric fission barrier was deduced to be within the range of $B_{f,a}$=4.0–4.9 MeV as shown in Fig. 10(b).

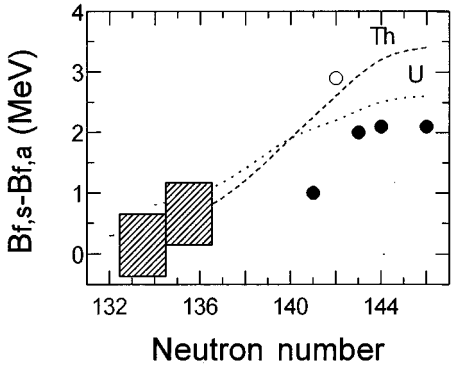

FIG. 11. The difference of the fission barriers between symmetric ($B_{f,s}$) and asymmetric fission ($B_{f,a}$) as a function of neutron number of the fissioning nuclei. The open circle and the solid circles are experimental data for the p + ^{232}Th and the p + ^{233,235,236,238}U [37,14], respectively. The dashed and dotted curves are theoretical values for even-even isotopes of Th and U, respectively [13].

The values of the difference between symmetric and asymmetric fission barrier heights ($\Delta B=E_{f,s}-E_{f,s}$) thus deduced are shown in Fig. 11 (cross-hatched area) as a function of neutron number of the compound nuclei of Pa isotopes (open circle) and Np ones (solid circles) together with the data in [37,14]. The fissioning nucleus is not determined in the present experiment but the first and second chance fission are predominant according to the statistical model calculation. The difference between the two barrier heights ΔB of about 0.5 MeV in the two reactions (^{16}O + ^{209}Bi and ^{18}O + ^{209}Bi), is in good agreement with the tendency of the theoretical calculations of static second potential barriers, one with reflection symmetry with respect to the plane perpendicular to the elongation axis and the other with reflection asymmetry as shown in Fig. 11 for even-even isotopes of Th (dashed line) and U (dotted line) [13]. (Because of the specification energy which is believed to be inherent for the fission of odd-A and odd-odd nuclides, the theoretical results for even-even nuclides may not be suitable for comparison with experimental results for odd-Z nuclides.)

Recently, low energy fission of neutron-deficient isotopes ($Z=89$–92) has been investigated by use of the secondary radioactive beam produced by projectile fragmentation of relativistic ^{238}U beams [20]. From their experiments, it is suggested that the transition from the symmetric to the asymmetric fission occurs at around $N=138$. However, the present result shows that the symmetric fission barrier is higher than the asymmetric one even for $N=134$ and 136 in the fission of protactinium $Z=91$.

The EC delayed fission of ^{228}Np, corresponding to the fission of ^{228}U ($N=136$) at an excited state of only a few MeV (most of the fission events observed are probably subbarrier events: $Q_{\mathrm{EC}}\cong 4.4$ MeV and $B_f=4.9$ MeV according to the theoretical predictions [52,53]) was studied and found to be mainly asymmetric in mass division [19]. This result suggests that the asymmetric barrier is lower than the symmetric one in the fission process of ^{228}U and it is consistent with the present result.

Finally, it is to be noted that the ''*extra energy*'' required for symmetric fission can be interpreted as the difference of the symmetric and asymmetric fission barrier height as done in this paper or as the additional energy required to go over the potential ridge from the asymmetric valley to the symmetric during the descent from the saddle to scission.

IV. CONCLUSIONS

The asymmetric mass division components have been observed in the fission reactions of ^{16}O + ^{209}Bi and ^{18}O + ^{209}Bi, the compound nuclei being ^{225}Pa ($N=134$) and ^{227}Pa ($N=136$). The fission barriers for the symmetric and the asymmetric mass division have been deduced from the observed incident energy dependence of symmetric and asymmetric mass yields with the statistical calculations. The symmetric barrier was found slightly higher than the asymmetric one in this region of light actinides. The difference between the two barrier heights in the fission of the present protactinium nuclides ($N\sim 135$) is considerably smaller compared with that in the neutron-rich nuclides of ^{233}Pa ($N\sim 142$). This indicates that the difference between the two barriers strongly depends on the neutron number of the fissioning nuclide.

ACKNOWLEDGMENTS

The authors are grateful to the staff of the nuclear chemistry and physics groups of Japan Atomic Energy Research Institute (JAERI), and wish to acknowledge the crew of the JAERI Tandem Accelerator and Institute for Nuclear Study (INS) SF Cyclotron for the accelerator operation.

[1] R. C. Jensen and A. W. Fairhall, Phys. Rev. **109**, 942 (1958).
[2] E. Konecny, H. J. Specht, and J. Weber, *Proceedings of the Third IAEA Symposium on the Physics and Chemistry of Fission*, Rochester, 1973 (IAEA, Vienna, 1974), Vol. 2, p. 3.
[3] M. G. Itkis, V. N. Okolovich, and G. N. Smirenkin, Nucl. Phys. **A502**, 243c (1989).
[4] J. P. Balagna, G. P. Ford, D. C. Hoffman, and J. P. Knight, Phys. Rev. Lett. **26**, 145 (1971).
[5] D. C. Hoffman and M. R. Lane, Radiochim. Acta **70/71**, 135 (1995).
[6] E. K. Hulet, J. F. Wild, R. J. Dougan, R. W. Lougheed, J. H. Landrum, A. D. Dougan, M. Schädel, R. L. Hahn, P. A. Baisden, C. M. Henderson, R. J. Dupzyk, K. Sümmerer, and G. R. Bethune, Phys. Rev. Lett. **56**, 313 (1986).
[7] T. Ohtsuki, Y. Nagame, H. Ikezoe, K. Tsukada, K. Sueki, and H. Nakahara, Phys. Rev. Lett. **66**, 17 (1991).
[8] Y. Nagame, I. Nishinaka, K. Tsukada, Y. Oura, S. Ichikawa, H. Ikezoe, Y. L. Zhao, K. Sueki, H. Nakahara, M. Tanikawa, T. Ohtsuki, H. Kudo, Y. Hamajima, K. Takamiya, and Y. H. Chung, Phys. Lett. B **387**, 26 (1996).
[9] A. Turkevich and J. B. Niday, Phys. Rev. **84**, 52 (1951).
[10] E. Konecny and H. W. Schmitt, Phys. Rev. **172**, 1213 (1968).
[11] H. C. Britt, H. E. Wegner, and J. C. Gursky, Phys. Rev. **129**, 2239 (1963).
[12] H. C. Britt and S. L. Whetstone, Jr., Phys. Rev. **133**, B603 (1964).
[13] P. Möller, Nucl. Phys. **A192**, 529 (1972).
[14] T. Ohtsuki, H. Nakahara, and Y. Nagame, Phys. Rev. C **48**, 1667 (1993).
[15] D. C. Hoffman, D. M. Lee, K. E. Gregorich, M. J. Nurmia, R. B. Chadwick, K. B. Chen, K. R. Czerwinski, C. M. Gannett, H. L. Hall, R. A. Henderson, B. Kadkhodayan, S. A. Kreek, and J. D. Leyba, Phys. Rev. C **41**, 631 (1990).
[16] P. Schillebeeckx, C. Wagemans, A. J. Deruytter, and R. Barthélémy, Nucl. Phys. **A545**, 623 (1992).
[17] H. L. Hall, K. E. Gregorich, R. A. Henderson, C. M. Gannett, R. B. Chadwick, J. D. Leyba, K. R. Czerwinski, B. Kadkhodayan, S. A. Kreek, D. M. Lee, M. J. Nurmia, D. C. Hoffman, C. E. A. Palmer, and P. A. Baisden, Phys. Rev. C **41**, 618 (1990).
[18] H. L. Hall, K. E. Gregorich, R. A. Henderson, C. M. Gannett, R. B. Chadwick, J. D. Leyba, K. R. Czerwinski, B. Kadkhodayan, S. A. Kreek, N. J. Hannink, D. M. Lee, M. J. Nurmia, D. C. Hoffman, C. E. A. Palmer, and P. A. Baisden, Phys. Rev. C **42**, 1480 (1990).
[19] S. A. Kreek, H. L. Hall, K. E. Gregorich, R. A. Henderson, J. D. Leyba, K. R. Czerwinski, B. Kadkhodayan, M. P. Neu, C. D. Kacher, T. M. Hamilton, M. R. Lane, E. R. Sylwester, A. Türler, D. M. Lee, M. J. Nurmia, and D. C. Hoffman, Phys. Rev. C **50**, 2288 (1994).
[20] K.-H. Schmidt, A. Heinz, H.-G. Clerc, B. Blank, T. Brohm, S. Czajkowski, C. Donzaud, H. Geissel, E. Hanelt, H. Irnich, M. C. Itkis, M. de Jong, A. Junghans, A. Magel, G. Münzenberg, F. Nickel, M. Pfützner, A. Piechaczek, C. Röhl, C. Scheidenberger, W. Schwab, S. Steinhäuser, K. Sümmerer, W. Trinder, B. Voss, and S. V. Zhdanov, Phys. Lett. B **325**, 313 (1994).
[21] M. R. Lane, K. E. Gregorich, D. M. Lee, M. F. Mohar, M. Hsu, C. D. Kacher, B. Kadkhodayan, M. P. Neu, N. J. Stoyer, E. R. Sylwester, J. C. Yang, and D. C. Hoffman, Phys. Rev. C **53**, 2893 (1996).
[22] E. K. Hulet, J. F. Wild, R. J. Dougan, R. W. Lougheed, J. H. Landrum, A. D. Dougan, P. A. Baisden, C. M. Henderson, R. J. Dupzyk, R. L. Hahn, M. Schädel, K. Sümmerer, and G. R. Bethune, Phys. Rev. C **40**, 770 (1989).

[23] J. F. Wild, E. K. Hulet, R. W. Lougheed, K. J. Moody, B. B. Bandong, R. J. Dougan, and A. Veeck, J. Alloys Compd. **213/214**, 86 (1994).
[24] T. M. Hamilton, E. K. Gregorich, D. M. Lee, K. R. Czerwinski, N. J. Hannink, C. D. Kacher, B. Kadkhodayan, S. A. Kreek, M. J. Nurmia, M. R. Lane, M. P. Neu, A. Türler, and D. C. Hoffman, Phys. Rev. C **46**, 1873 (1992).
[25] E. K. Hulet, R. W. Lougheed, J. H. Landrum, J. F. Wild, D. C. Hoffman, J. Weber, and J. B. Wilhelmy, Phys. Rev. C **21**, 966 (1980).
[26] W. John, E. K. Hulet, R. W. Lougheed, and J. J. Wesolowski, Phys. Rev. Lett. **27**, 45 (1971).
[27] J. P. Unik, J. E. Gindler, L. E. Glendenin, K. F. Flynn, A. Gorski, and R. K. Sjoblom, *Proceedings of the Third IAEA Symposium on the Physics and Chemistry of Fission*, [2], Vol. 2, p. 19.
[28] D. Hoffman, D. Lee, A. Ghiorso, M. Nurmia, and K. Aleklett, Phys. Rev. C **22**, 1581 (1980).
[29] D. C. Hoffman, J. B. Wilhelmy, J. Weber, W. R. Daniels, E. K. Hulet, R. W. Lougheed, J. H. Landrum, J. F. Wild, and R. J. Dupzyk, Phys. Rev. C **21**, 972 (1980).
[30] S. D. Beĭzin, S. V. Zhdanov, M. G. Itkis, V. N. Okolovich, G. N. Smirenkin, and M. I. Subbotin, Sov. J. Nucl. Phys. **53**, 411 (1991).
[31] I. D. Alkhazov, S. S. Kovalenko, O. I. Kostochkin, L. Z. Malkin, K. A. Petrzhak, and V. I. Shpakov, Sov. J. Nucl. Phys. **15**, 12 (1972).
[32] A. A. Goverdovskiĭ and V. F. Mitrofanov, Phys. At. Nucl. **56**, 24 (1993).
[33] E. Allaert, C. Wagemans, G. Wegener-Penning, A. Deruytter, and R. Barthélémy, Nucl. Phys. **A380**, 61 (1982).
[34] E. Pfeiffer, Z. Phys. **240**, 403 (1970).
[35] J. Weber, H. C. Britt, A. Gavron, E. Konecny, and J. B. Wilhelmy, Phys. Rev. C **13**, 2413 (1976).
[36] T. Ohtsuki, Y. Nagame, K. Tsukada, N. Shinohara, S. Baba, K. Hashimoto, I. Nishinaka, K. Sueki, Y. Hatsukawa, K. Hata, T. Sekine, I. Kanno, H. Ikezoe, and H. Nakahara, Phys. Rev. C **44**, 1405 (1991).
[37] H. Kudo, H. Muramatsu, H. Nakahara, K. Miyano, and I. Kohno, Phys. Rev. C **25**, 3011 (1982).
[38] E. A. C. Crouch, At. Data Nucl. Data Tables **19**, 417 (1977).
[39] M. P. Menon and P. K. Kuroda, J. Inorg. Nucl. Chem. **26**, 401 (1964).
[40] S. B. Manohar, P. P. Venkatesan, S. M. Deshmukh, S. Prakash, and M. V. Ramaniah, Phys. Rev. C **19**, 1827 (1979).
[41] E. F. Neuzil and A. W. Fairhall, Phys. Rev. **129**, 2705 (1963).
[42] J. Davit Bowman and R. H. Heffner, Nucl. Instrum. Methods **148**, 503 (1978).
[43] F. Busch, W. Pfeffer, B. Kohlmeyer, D. Schüll, and F. Pühlhoffer, Nucl. Instrum. Methods **171**, 71 (1980).
[44] S. B. Kaufman, E. P. Steinberg, B. D. Wilkins, J. Unik, A. J. Gorski, and M. J. Fluss, Nucl. Instrum. Methods **115**, 47 (1974).
[45] H.-O. Neidel and H. Henschel, Nucl. Instrum. Methods **178**, 137 (1980).
[46] A. H. Wapstra, G. Audi, and R. Hoekstra, At. Data Nucl. Data Tables **39**, 290 (1988).
[47] V. E. Viola, K. Kwiatkowski, and M. Walker, Phys. Rev. C **31**, 1550 (1985).
[48] Arthur C. Wahl, At. Data Nucl. Data Tables **39**, 1 (1988).
[49] J. P. Bocquet and R. Brissot, Nucl. Phys. **A502**, 213c (1989).
[50] A. Gavron, H. C. Britt, P. D. Goldstone, J. B. Wilhelmy, and S. E. Larsson, Phys. Rev. Lett. **38**, 1457 (1977).
[51] A. J. Sierk, Phys. Rev. C **33**, 2039 (1986).
[52] P. Möller and J. R. Nix, Nucl. Phys. **A229**, 269 (1974).
[53] P. Möller and J. R. Nix, At. Data Nucl. Data Tables **39**, 290 (1988).